ARTICLES

Recurrent variational approach to the two-leg Hubbard ladder

Eugene H. Kim
Department of Physics, University of California, Santa Barbara, California 93106-9530

Germán Sierra
Instituto de Matemáticas y Física Fundamental, C.S.I.C., 28006 Madrid, Spain

Daniel Duffy
Department of Physics, University of California, Santa Barbara, California 93106-9530

(Received 9 February 1999)

We applied the recurrent variational approach to the two-leg Hubbard ladder. At half filling, our variational ansatz was a generalization of the resonating valence-bond state. At finite doping, hole pairs were allowed to move in the resonating valence-bond background. The results obtained by the recurrent variational approach were compared with results from density matrix renormalization group. [S0163-1829(99)00332-X]

I. INTRODUCTION

In the hope to get a better understanding of strongly interacting systems, there has been considerable interest in ladder systems.[1] These ladder systems have proven to be a theoretical wonderland, both analytically[2] and numerically.[3] However, much of the analytic work done on ladders has been in weak coupling (or perturbatively in some parameter), namely because there are very few analytic methods at strong coupling. Exact diagonalization, Monte Carlo, and density matrix renormalization group methods have been the primary tools for studying these systems at strong coupling. Each of these methods has both strengths and weaknesses when considering the lattice sizes, temperatures, and couplings one can consider.

With the ability to fabricate these materials,[4] ladders are not just a theoretical playground. For example, in $(VO)_2P_2O_7$, there are well separated two-leg ladders composed of VO_4.[5] Also, the cupratelike material $SrCu_2O_3$ consists of weakly coupled CuO_2 two-leg ladders,[6] and the material $Sr_2Cu_3O_5$ consists of weakly coupled CuO_2 three-leg ladders.[7]

Recently, a powerful analytic method was developed to deal with strongly coupled quasi-one-dimensional systems—the recurrent variational approach (RVA).[8–10] This method is similar in spirit to Wilson's numerical renormalization group[11] and White's density matrix renormalization group (DMRG).[12] The key idea in all of these methods is to build up the system by adding on sites at the boundary. However, the real power of the RVA is that, though analytic, the physics of the problem is taken into account in an unbiased way and elucidated quite clearly. For example, the importance of different configurations in the ground-state wave function is determined without any outside assumptions, and the physics of these configurations is made clear. For a review of the RVA, see Ref. 10.

In this paper, we apply the RVA to the two-leg Hubbard ladder at strong coupling and small dopings. Though a considerable amount of work has been done on the Hubbard ladder and many of its properties are known, we are unaware of any work that has put this information together and constructed a ground-state wave function. Our goal in this paper is to provide a simple physical picture of what the ground state might look like and to go ahead and construct a ground-state wave function.

The Hamiltonian of the two-leg Hubbard ladder is given by

$$H=-t\sum_{\mathbf{i},s}\ (c^{\dagger}_{\mathbf{i},s}c_{\mathbf{i}+\hat{\mathbf{x}},s}+\text{h.c.})-t_{\perp}\sum_{\mathbf{i},s}\ (c^{\dagger}_{\mathbf{i},s}c_{\mathbf{i}+\hat{\mathbf{y}},s}+\text{H.c.})$$

$$+U\sum_{\mathbf{i}}\ n_{\mathbf{i},\uparrow}n_{\mathbf{i},\downarrow}\,, \tag{1}$$

where $c^{\dagger}_{\mathbf{i},s}$ creates a fermion at site $\mathbf{i}$ with spin s, $n_{\mathbf{i},s}=c^{\dagger}_{\mathbf{i},s}c_{\mathbf{i},s}$, t is the hopping matrix element along the chain, $t_{\perp}$ is the hopping matrix element perpendicular to the chain (i.e., along the rung), and U is the on-site Coulomb repulsion. Site $\mathbf{i}$ has coordinates (x,y) with $1\leqslant x\leqslant N$ and $y=1,2$. It will also be convenient to introduce the following two operators:

$$\Delta^{\dagger}_{\mathbf{i},\mathbf{j}}=c^{\dagger}_{\mathbf{i},\uparrow}c^{\dagger}_{\mathbf{j},\downarrow}+c^{\dagger}_{\mathbf{j},\uparrow}c^{\dagger}_{\mathbf{i},\downarrow}\,, \tag{2}$$

which creates a singlet across sites $\mathbf{i}$ and $\mathbf{j}$, and

$$D^{\dagger}_{\mathbf{i}}=c^{\dagger}_{\mathbf{i},\uparrow}c^{\dagger}_{\mathbf{i},\downarrow}\,, \tag{3}$$

which creates a doubly occupied site.

The rest of the paper is organized as follows. In Sec. II, we consider the half-filled case. In Sec. III, we consider the Hubbard ladder at small dopings. In Sec. IV, we present our results for the ground-state energies and compare with

DMRG. Finally, in Sec. V we summarize our results and present some concluding remarks.

II. HALF-FILLED HUBBARD LADDER

We begin with the half-filled ladder. What are the ingredients necessary to construct a wave function that captures the physics of the half-filled Hubbard ladder? A trail of clues has been laid by previous works. First of all, we know that at strong coupling the half-filled Hubbard model is equivalent to the Heisenberg model. Secondly, it is known that the two-leg Heisenberg ladder (and Hubbard ladder) have a spin gap and short-range spin correlations. Furthermore, it has been shown that the resonating valence bond (RVB) state captures the essential physics of the two-leg Heisenberg ladder.[13,8] Hence, the RVB picture should capture the essential physics of the half-filled Hubbard ladder at strong coupling. Thus, we propose a generalization of the RVB state as our variational ansatz.

A key property of the RVB state is that it is the exact solution to the 2×2 Heisenberg plaquette. Therefore, we base our generalized RVB state on the exact solution to the 2×2 Hubbard plaquette. Since the 2×2 plaquette will serve as the basis for our ansatz, we discuss it in detail below.

It should be noted that the 2×2 plaquette has been the basis for other work.[14–16] In these approaches, the ladder is first broken up into plaquettes and each plaquette is diagonalized. Then some method (contractor renormalization group,[14] exact diagonalization,[15] or perturbation theory[16]) is used to essentially ''glue'' the plaquettes back together into a ladder. These approaches, especially Refs. 14 and 15, are similar to the real-space renormalization group methods that have been used on lattice models.[17]

In our approach we do *not* break up the ladder into plaquettes; rather, we use the 2×2 plaquette as a way to generalize the RVB state for the Hubbard model. The RVB state for the Heisenberg model is a nonperturbative state, which is (lattice) translationally invariant and consists of singlets between all pairs of nearest-neighbor sites. Our generalized RVB state is also a nonperturbative, (lattice) translationally invariant state consisting of singlets between all pairs of nearest-neighbor sites. However, our generalized RVB state for the Hubbard model also includes doubly occupied sites. In the Heisenberg model, these doubly occupied states have already been integrated out, giving an effective spin-spin interaction J. The key idea of our approach is that, using the 2×2 plaquette, the RVB and generalized RVB states can be generated *recursively*. (This will be discussed in more detail below.)

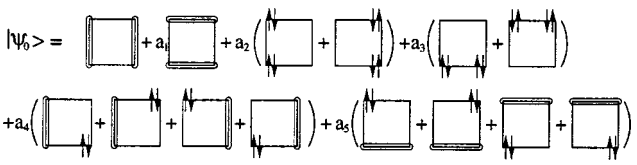

FIG. 1. Ground-state wave function for the 2×2 half-filled plaquette. A circled link represents a singlet bond. (See text for a full explanation of each state.)

TABLE I. Values of the parameters for the half-filled 2×2 plaquette (with $t=t_\perp=1$), which give the exact ground state.

U	a_1	a_3	a_5	a_2	a_4
8	-1.0	-0.0762	-0.3306	$-a_3$	$-a_5$
16	-1.0	-0.0221	-0.1807	$-a_3$	$-a_5$
24	-1.0	-0.0101	-0.1229	$-a_3$	$-a_5$

A. The 2×2 Plaquette

The ground state of the 2×2 plaquette is given by

$$|\psi_0\rangle=|\varphi_0\rangle+a_1\ |\varphi_1\rangle+a_2\ |\varphi_2\rangle+a_3\ |\varphi_3\rangle +a_4\ |\varphi_4\rangle+a_5\ |\varphi_5\rangle, \tag{4}$$

where

$$\begin{aligned}
|\varphi_0\rangle&=\Delta^\dagger_{(1,1),(1,2)}\Delta^\dagger_{(2,1),(2,2)}|0\rangle,\\
|\varphi_1\rangle&=\Delta^\dagger_{(1,1),(2,1)}\Delta^\dagger_{(1,2),(2,2)}|0\rangle,\\
|\varphi_2\rangle&=D^\dagger_{(1,1)}D^\dagger_{(1,2)}|0\rangle+D^\dagger_{(2,1)}D^\dagger_{(2,2)}|0\rangle,\\
|\varphi_3\rangle&=D^\dagger_{(1,1)}D^\dagger_{(2,1)}|0\rangle+D^\dagger_{(1,2)}D^\dagger_{(2,2)}|0\rangle,\\
|\varphi_4\rangle&=\Delta^\dagger_{(1,1),(1,2)}D^\dagger_{(2,1)}|0\rangle+\Delta^\dagger_{(1,1),(1,2)}D^\dagger_{(2,2)}|0\rangle\\
&\quad+\Delta^\dagger_{(2,1),(2,2)}D^\dagger_{(1,1)}|0\rangle+\Delta^\dagger_{(2,1),(2,2)}D^\dagger_{(1,2)}|0\rangle,\\
|\varphi_5\rangle&=\Delta^\dagger_{(1,1),(2,1)}D^\dagger_{(1,2)}|0\rangle+\Delta^\dagger_{(1,1),(2,1)}D^\dagger_{(2,2)}|0\rangle\\
&\quad+\Delta^\dagger_{(1,2),(2,2)}D^\dagger_{(1,1)}|0\rangle+\Delta^\dagger_{(1,2),(2,2)}D^\dagger_{(2,1)}|0\rangle.
\end{aligned} \tag{5}$$

$|\psi_0\rangle$ is shown schematically in Fig. 1.

We will be mainly interested in the case $t=t_\perp$. In Table I we list the values of the parameters for several values of U (with $t=t_\perp=1$).

Notice that the solution to the 2×2 plaquette (with $t=t_\perp$) has D_4 symmetry. (D_4 is the symmetry group of the square.) However, the ground state does *not* transform in the scalar representation of D_4; it transforms in the B_2 representation of D_4. (B_2 is the one-dimensional representation that changes sign upon rotation by 90° and reflection about the diagonals.) B_2 coincides with the standard $d_{x^2-y^2}$ symmetry. The B_2 representation is what forbids some configurations, as those shown in Fig. 2, from appearing in the ground-state wave function.

A few more words are in order about the ground-state wave function. Notice that $a_1=-1$ [i.e., the weight of the horizontal singlets is equal to (minus) the weight of the vertical singlets]. This is the RVB mechanism–the system lowers its energy by resonating between horizontal and vertical singlets; a_1 is the ''RVB parameter.'' Also, notice that $|a_2|,|a_3|=\mathcal{O}(a_4^2)$. This will play a role in constructing the ansatz for the half-filled ladder.

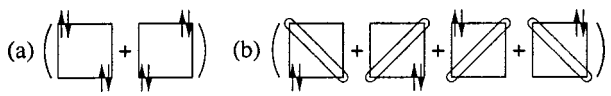

FIG. 2. States that the B_2 representation prevents from appearing in the ground-state wave function of the half-filled plaquette.

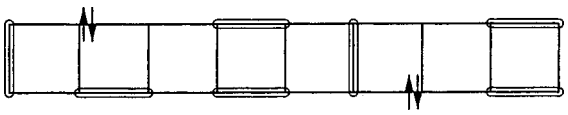

FIG. 3. Typical configuration appearing in the ground-state wave function of the half-filled ladder.

B. The Ladder

In the approximation where we use the configurations of the 2×2 plaquette as the basis of our ansatz, a typical configuration for the ladder is shown in Fig. 3. Within this approximation, the ground state will still be a superposition of all possible configurations of the type shown in Fig. 3. Therefore, it seems like working with this kind of state will be a formidable task. Fortunately, the RVA gives us a straightforward way of dealing with such a state–generate it *recursively*. Specifically, the RVA builds the ground state of a ladder with $N+\nu$ rungs using the knowledge of the ground states of a ladder with $N, N+1, \ldots, N+\nu-1$ rungs. This is achieved by recursion relations that express the ground state $|N+\nu\rangle$ in terms of the ground states $\{|N+i\rangle\}$ with $i=0,\ldots,\nu-1$.[8,10]

Using these ingredients, we consider the following ansatz for the half-filled Hubbard ladder

$$\begin{aligned}|N+2\rangle &= |\phi_0\rangle_{N+2}|N+1\rangle+\alpha|\phi_1\rangle_{N+2}|N+1\rangle\\ &+\beta|\phi_2\rangle_{N+1,N+2}|N\rangle+\gamma|\phi_3\rangle_{N+1,N+2}|N\rangle\\ &+\xi|\phi_4\rangle_{N+1,N+2}|N\rangle+\eta|\phi_5\rangle_{N+1,N+2}|N\rangle\\ &+\delta|\phi_6\rangle_{N,N+1,N+2}|N-1\rangle\\ &+\varepsilon|\phi_7\rangle_{N,N+1,N+2}|N-1\rangle,\end{aligned} \tag{6}$$

which is shown schematically in Fig. 4.[18] For completeness, the states in terms of the operators in Eqs. 2 and 3 are given in Appendix A.

A few words are in order about the configurations in our ansatz. (i) β, the weight of the horizontal bond (relative to the vertical bond), is the ''RVB parameter.'' For a true RVB state, we would have $\beta=-1$. Although we do not expect $\beta=-1$, from work on the Heisenberg model the variational parameters were shown to evolve smoothly with system size;[8] we expect $|\beta|=\mathcal{O}(1)$. (ii) Suppose we iterate the recursion relations once. Then $|\phi_0\rangle$ and $|\phi_1\rangle$ (and also $|\phi_5\rangle$) generate the terms shown in Fig. 5. In the ground state of the 2×2 plaquette, the states in Fig. 5(b) have weight $\mathcal{O}(\alpha)$, the states in Fig. 5(c) have weight $\mathcal{O}(\alpha^2)$, and the states in Fig. 5(d) do not appear. Since we expect the parameters to evolve smoothly,[8] we expect $\eta\approx-\alpha^2$. (η is behaving as a ''counter-term''; it's job is to subtract off the α^2 contribution from $|\phi_1\rangle$.) (iii) Even though we no longer have D_4 symmetry, initial calculations showed that the states in Fig. 2(b) do not appear in the ground state of the Hubbard ladder. (This is another indication that the parameters evolve smoothly from the 2×2 case to the ladder.) Therefore, we do not consider them in what follows. (iv) Since the configurations $|\phi_6\rangle_{N,N+1,N+2}$ and $|\phi_7\rangle_{N,N+1,N+2}$ appear as intermediate states for the resonances shown in Fig. 6, it is necessary to include these states in the ansatz to give us an RVB state. This can easily be seen by comparing the weights of the coefficients as shown in Table II (see below).

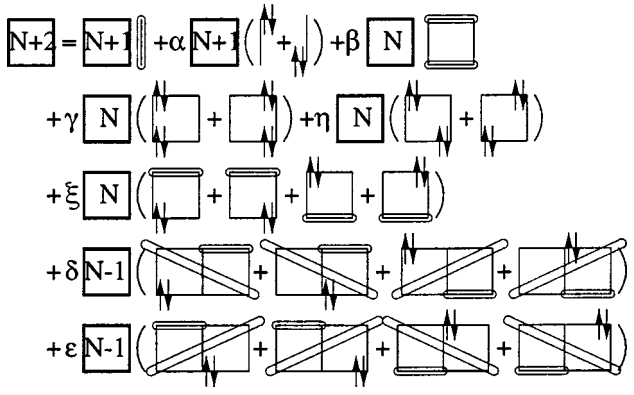

FIG. 4. The RVA ansatz for the half-filled Hubbard ladder. Note that links or sites connected with a circle represent a singlet bond.

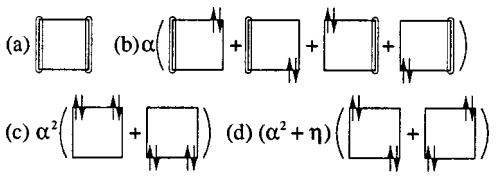

FIG. 5. States generated by $|\phi_0\rangle$ and $|\phi_1\rangle$ (and also $|\phi_5\rangle$) by running the recursion relations once.

In order to compute the values of the coefficients, we treat them as variational parameters and minimize the ground-state energy with respect to these parameters. The ground-state energy and other quantities appear as recursion relations. It will be useful to define

$$\begin{aligned}E_N&=\langle N|H_N|N\rangle,\\ D_N&=\langle N-1|_N\langle\phi_0|H_N|N\rangle,\\ C_N&=\langle N-1|_N\langle\phi_1|H_N|N\rangle,\\ Z_N&=\langle N|N\rangle,\\ Y_N&=\langle N-1|_N\langle\phi_0|N\rangle,\\ X_N&=\langle N-1|_N\langle\phi_1|N\rangle.\end{aligned} \tag{7}$$

They are supplemented by the initial conditions

$$\begin{aligned}&Z_0=1,\ Y_0=0,\ X_0=0,\\ &E_0=0,\ D_0=0,\ C_0=0.\end{aligned} \tag{8}$$

To determine the values for the variational parameters for a given (finite) value of N, we iterate the recursion relations and minimize the quantity E_N/Z_N numerically. The actual

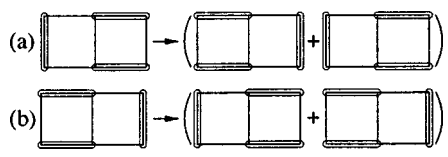

FIG. 6. Other ''resonances,'' which play an important role in the RVB picture.

recursion relations are quite unwieldly; we have relegated them, as well as their derivation, to Appendix A.

The values of the variational parameters for various values of U (with $t=t_\perp=1$) are shown in Table II. The results were obtained on a 2×32 ladder. Notice that (i) $|\beta|=\mathcal{O}(1)$, and we have produced an RVB state. (ii) $|\eta|=\mathcal{O}(\alpha^2)$, and η is indeed behaving as a counterterm. (iii) $|\delta|,|\varepsilon|\approx\alpha/3$. Therefore, these configurations are non-negligible, suggesting that the resonances shown in Fig. 6 are important to the RVB picture.

III. THE DOPED HUBBARD LADDER

Now, we consider the doped Hubbard ladder. In Ref. 9 it was shown that hole pairs moving through an RVB background captures the essential physics of the $t-J$ ladder at small dopings. Since the $t-J$ model is the large U limit of the Hubbard model, we expect this picture to hold for the Hubbard model at large U and small dopings. Therefore, we consider an ansatz of hole pairs moving through our generalized RVB background for the Hubbard ladder at small dopings.

Since the structure of the hole pairs is based on the exact solution to the 2×2 plaquette with 2 holes, we consider the 2×2 case in detail below.

A. The 2×2 Plaquete with Two Holes

The ground state of the 2×2 plaquette with 2 holes is given by

$$|\psi_0^h\rangle=|\varphi_0^h\rangle+b_1\ |\varphi_1^h\rangle+b_2\ |\varphi_2^h\rangle+b_3\ |\varphi_3^h\rangle, \tag{9}$$

where

$$\begin{aligned}
|\varphi_0^h\rangle&=\Delta^\dagger_{(1,1),(1,2)}|0\rangle+\Delta^\dagger_{(2,1),(2,2)}|0\rangle,\\
|\varphi_1^h\rangle&=\Delta^\dagger_{(1,1),(2,1)}|0\rangle+\Delta^\dagger_{(1,2),(2,2)}|0\rangle,\\
|\varphi_2^h\rangle&=\Delta^\dagger_{(1,1),(2,2)}|0\rangle+\Delta^\dagger_{(2,1),(1,2)}|0\rangle,
\end{aligned} \tag{10}$$

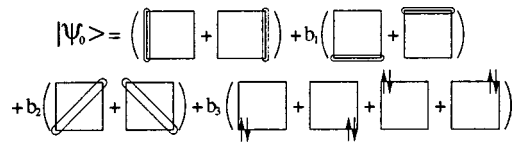

FIG. 7. Ground-state wave function for the 2×2 plaquette with two holes.

$$|\varphi_3^h\rangle=D^\dagger_{(1,1)}|0\rangle+D^\dagger_{(1,2)}|0\rangle+D^\dagger_{(2,1)}|0\rangle+D^\dagger_{(2,2)}|0\rangle.$$

$|\psi_0^h\rangle$ is shown schematically in Fig. 7.

In Table III we list the values of the parameters for several values of U (with $t=t_\perp=1$).

Notice that the solution to the 2×2 case (with $t=t_\perp$) has D_4 symmetry. However, now the ground state transforms in the *scalar* representation of D_4. Recalling that the ground state of the half-filled ladder transforms in the B_2 representation, we see that the operator that creates a hole pair out of the undoped system has $d_{x^2-y^2}$ symmetry.[19] These facts continue to be true for low doping in larger ladders. Also, notice that $b_3=\mathcal{O}(\alpha)$ where α is from the half-filled ladder. This will play a role in writing our ansatz for the doped ladder.

B. The Ladder

In the approximation where we use the configurations of the generalized RVB state as well as the hole pair configurations, a typical configuration for the doped ladder is shown in Fig. 8. In this approximation, the ground state will still be a superposition of all such configurations shown in Fig. 8. Fortunately, we can generate such a state *recursively*. Specifically, we build the ground state of a ladder with $N+\nu$ rungs and $P+\mu$ holes using the knowledge of the ground states of a ladder with $N,N+1,\ldots,N+\nu-1$ rungs and $P,P+1,\ldots,P+\mu$ holes. This is achieved by recursion relations that express the ground state $|N+\nu,P+\mu\rangle$ in terms of the ground states $\{|N+i,P+j\rangle\}$ with $i=0,\ldots,\nu-1$ and $j=0,\ldots,\mu$.[9,10]

Using the above ingredients, we consider the following ansatz for the doped Hubbard ladder

$$\begin{aligned}
|N+2\ \ P+1\rangle=&|\phi_0\rangle_{N+2}|N+1\ \ P+1\rangle+\alpha|\phi_1\rangle_{N+2}|N+1\ \ P+1\rangle+\beta|\phi_2\rangle_{N+1,N+2}|NP+1\rangle+\gamma|\phi_3\rangle_{N+1,N+2}|NP+1\rangle\\
&+\xi|\phi_4\rangle_{N+1,N+2}|NP+1\rangle+\eta|\phi_5\rangle_{N+1,N+2}|NP+1\rangle+\delta|\phi_6\rangle_{N,N+1,N+2}|N-1\ \ P+1\rangle\\
&+\varepsilon|\phi_7\rangle_{N,N+1,N+2}|N-1\ \ P+1\rangle+|\phi_0^h\rangle_{N+2}|N+1\ \ P\rangle+\lambda|\phi_1^h\rangle_{N+1,N+2}|NP\rangle+\zeta|\phi_2^h\rangle_{N+1,N+2}|NP\rangle\\
&+\mu|\phi_3^h\rangle_{N,N+1,N+2}|N-1\ \ P\rangle+\nu|\phi_4^h\rangle_{N,N+1,N+2}|N-1\ \ P\rangle,
\end{aligned} \tag{11}$$

which is shown schematically in Fig. 9. For completeness, the states in terms of the operators in Eqs. (2) and (3) are given in Appendix B.

A few words are in order about the configurations in our ansatz. (i) The ansatz contains the configurations for the RVB state, as well as the configurations for holes bound in pairs. The hole pair states are based on the exact solution to the 2×2 plaquette with 2 holes, and our ansatz reproduces this exact solution. (ii) The states $|\phi_3^h\rangle_{N,N+1,N+2}$ and $|\phi_4^h\rangle_{N,N+1,N+2}$ extend over three rungs. These states are necessary to allow the hole pairs to move smoothly through the RVB background. (iii) Note that physically, the picture of hole pairs moving through an RVB background can only be appropriate for low dopings.

To compute the values of the coefficients in our ansatz, we treat them as variational parameters and minimize the ground-state energy with respect to these parameters. It will be useful to define

TABLE II. Values of the variational parameters for a 2×32 half-filled ladder with $t=t_\perp=1$.

U	α	β	γ	ξ	η	δ	ε
8	.3296	−.8710	−.0782	−.2877	−.0938	.1031	.1031
16	.1848	−.8800	−.0243	−.1606	−.0299	.0639	.0639
24	.1265	−.8817	−.0113	−.1097	−.0142	.0451	.0451

$$
\begin{aligned}
E_{N,P}&=\langle NP|H_N|NP\rangle,\\
D_{N,P}&=\langle N-1\ \ P|_N\langle\phi_0|H_N|NP\rangle,\\
C_{N,P}&=\langle N-1\ \ P|_N\langle\phi_1|H_N|NP\rangle,\\
Z_{N,P}&=\langle NP|NP\rangle,\\
Y_{N,P}&=\langle N-1\ \ P|_N\langle\phi_0|NP\rangle,\\
X_{N,P}&=\langle N-1\ \ P|_N\langle\phi_1|NP\rangle.
\end{aligned}
\tag{12}
$$

They are supplemented by the initial conditions

$$
\begin{aligned}
&Z_{N,P=N}=1,\ Y_{N,P=N}=0,\ X_{N,P=N}=0,\\
&E_{N,P=N}=0,\ D_{N,P=N}=0,\ C_{N,P=N}=0,\\
&F_{N<P,P}=0\ \ \text{for}\ \ F=Z,Y,X,E,D,C.
\end{aligned}
\tag{13}
$$

To determine the values for the variational parameters for given (finite) values of N and P, we iterate the recursion relations and we minimize the quantity $E_{N,P}/Z_{N,P}$. The actual recursion relations are quite unwieldly; we have relegated them, as well as their derivation, to Appendix B.

What is the nature of the state we have constructed? In order to answer this question, we plot β, λ, and ζ vs doping. These parameters contain most of the physics of our ansatz. β is the ''RVB parameter''; λ and ζ are the weights of the hole pair configurations. The results were obtained on a 2×32 ladder.

First, consider Fig. 10(a). β begins at $\mathcal{O}(-1)$ and increases (i.e., becomes less negative) with doping until a critical doping, x_c, where it vanishes. Beyond this doping, β is positive. This has also been found for the $t-J$ ladder.[9] Upon doping, the hole pairs cause destructive interference which degrades the RVB mechanism. For $x>x_c$, this destructive interference has driven β positive, and it is no longer appropriate to think of our state as describing hole pairs moving through an RVB background.[9]

Similar to the t-J ladder, the difference between $x<x_c$ and $x>x_c$ can be attributed to two different internal structures of the hole pairs. For $x<x_c$, the hole pairs have a

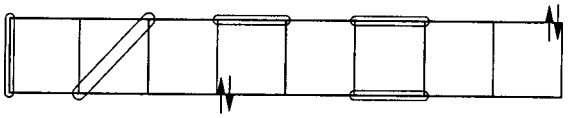

FIG. 8. Typical configuration appearing in the ground-state wave function of the doped ladder.

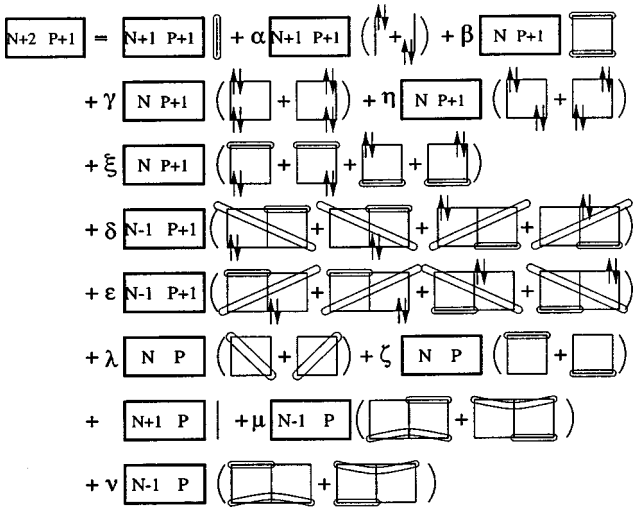

FIG. 9. The RVA ansatz for the doped Hubbard ladder.

$d_{x^2-y^2}$ structure *relative* to the RVB background. For $x>x_c$, the hole pairs have an s-wave-like symmetry relative to their background.[9]

Now, consider Figs. 10(b) and 10(c). First of all, notice that $\lambda>\zeta$. This shows the importance of the diagonal frustrating bonds for all dopings.[20] Also, notice that λ and ζ both reach their maximum at $x=\frac{1}{2}$. At $x=\frac{1}{2}$ the system is essentially a large scale reproduction of the 2×2 plaquette with 2 holes.[9] Indeed, the values of λ and ζ at $x=\frac{1}{2}$ are similar to their values for the 2×2 plaquette.

IV. GROUND-STATE ENERGIES

First, we show results for energy per site vs U in Fig. 11. For comparison, DMRG results are presented for the same set of parameters. In our DMRG runs, we kept up to 300 states with a maximum discarded weight of 1.88×10^{-4} for $U=4$; all higher values of U had lower discarded weights.[21]

At half-filling, as we would expect, our ansatz is most accurate for large U and large $t_\perp$. The ground-state energy per site for a 2×32 half-filled ladder as a function of U for various $t_\perp$ is shown in Fig. 11(a). For $U=8$ and $t_\perp=1$, the energy from the RVA agrees with DMRG to within 90% and improves as U or $t_\perp$ is increased. Up to about $U=10$, longer bonds (extending over at least 3 rungs) are coming into play. These states should be included in the ansatz to further improve the overlap with the ground state. At $U=16$ and $t_\perp=1$, our ansatz gives a ground-state energy within 94% of the DMRG result.

It should be noted that for the Heisenberg ladder, the RVB state gives a ground-state energy within 96% of true ground-state energy, obtained from DMRG.[8] A recent

TABLE III. Values of the parameters for the 2×2 plaquette with two holes (with $t=t_\perp=1$), which gives the exact ground state.

U	b_1	b_2	b_3
8	1.0	1.2470	0.3569
16	1.0	1.3131	0.2100
24	1.0	1.3420	0.1483

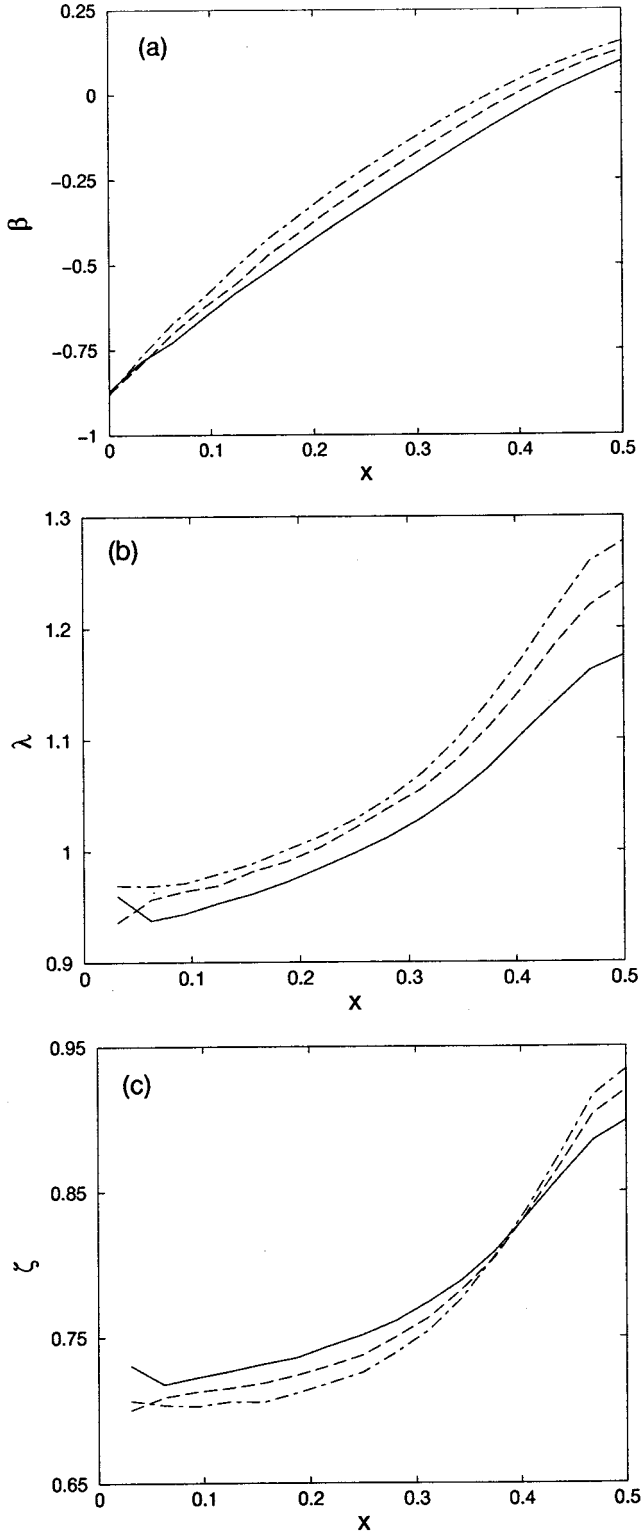

FIG. 10. (a) β vs doping, x, for a 2×32 ladder at $U=8$ (solid line), $U=12$ (dashed line), and $U=16$ (dashed-dotted line). (b) Same as (a) for λ. (c) Same as (a) for ζ.

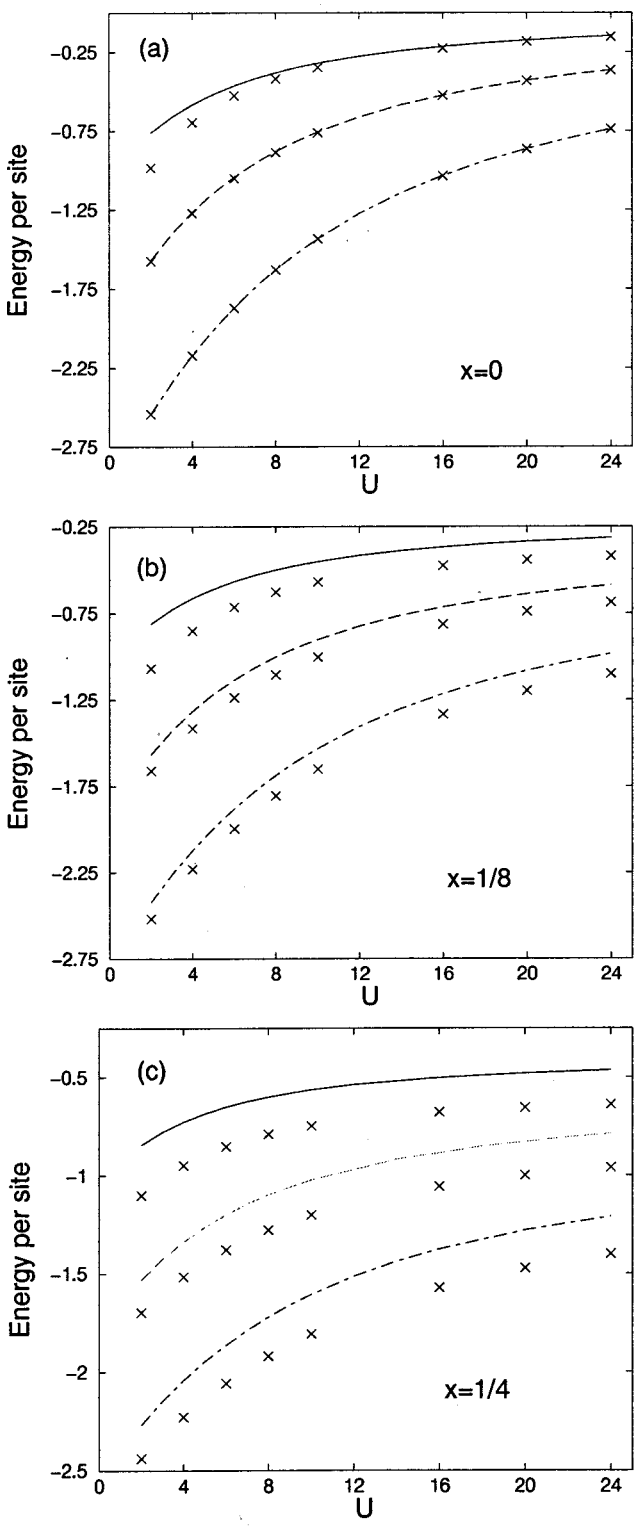

FIG. 11. (a) Ground-state energy per site at half filling ($x=0$) vs U for $t_\perp=1$ (solid line), $t_\perp=2$ (dashed line), $t_\perp=3$ (dashed-dotted line). For comparison, DMRG results (shown as $\times$) are presented for the same set of parameters. (b) Same as (a) except for $x=\frac{1}{8}$. (c) Same as (a) except for $x=\frac{1}{4}$.

DMRG study of different ladder models found that the Hubbard model and Heisenberg model begin to agree only for rather large U ($U\approx16$).[22] Therefore, it is not surprising that the RVB picture becomes as good for the Hubbard model as it is for the Heisenberg model at $U\approx16$.

Figure 11(b) shows the ground-state energy of the RVA ansatz as a funtion of U for various $t_\perp$ for a doping of $x=\frac{1}{8}$ on a 2×32 ladder. Again, we show energies obtained from DMRG for the same set of parameters. For $U=16$ and $t_\perp=1$, the two energies agree to only within 77% and improves slightly as $t_\perp$ is increased. For example, at $U=16$ and $t_\perp=2$, the overlap of energies increases to 87%. Further dis-

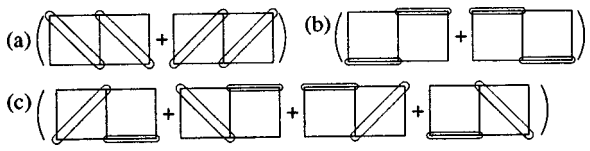

FIG. 12. ''Pair-breaking'' configurations that are playing a rather large role in the ground state of the doped Hubbard ladder.

crepancies occur when the doping is increased to $x=1/4$ [see Fig. 11(c)].

The differences in ground-state energies occur due to the importance of ''pair-breaking'' configurations, like those shown in Fig. 12. The weights of these types of states increase as we move away from half-filling. Consequently, to further improve the RVA ansatz, such states must be included in the wave function. Note also that our ansatz would be essentially exact for the case where hole pairs are well localized on a rung. For the $t-J$ model with $J_{rung} \gg J_{chain}, t$, pairs are well localized along a rung, and the ground state is essentially a product of rung singlets and rung hole pairs. However, for the Hubbard model at strong coupling (i.e., $U \gg t_\perp, t$), this is not the case. Holes would always rather occupy *adjacent* rungs, even for $t_\perp \gg t$, since this minimizes the Coulomb energy from doubly occupied sites. To see this consider a 2×2 plaquette with 2 holes; let $t \ll t_\perp$ and $t, t_\perp \ll U$. With 1 particle on each rung (i.e., one hole on each rung), the ground-state energy is approximately $-2t_\perp$; with both particles on the same rung (i.e., both holes on the same rung), the ground-state energy is approximately $-J=-4t_\perp^2/U$. Therefore, at large U, the particles would rather occupy adjacent rungs. (See Fig. 13.)

The situation we have with the doped ladder is similar to what we had for the half-filled ladder in the early stages of this paper. We found that without the states $|\phi_6\rangle$ and $|\phi_7\rangle$, which extend over three rungs (see Fig. 4), the RVA did not accurately reproduce the ground state even at extremely large U. However, once we included $|\phi_6\rangle$ and $|\phi_7\rangle$, the results from the RVA improved drastically. Based on these results, we expect the RVA to greatly improve by including the states shown in Fig. 12.

In Fig. 14, we plot energy per site vs doping for a 2×32 ladder for $U=8$ and $U=16$ (with $t_\perp=1$) in order to better understand the region of validity of our RVA ansatz. Again, we see good agreement with DMRG results at half filling. However, as soon as we dope, configurations like those shown in Fig. 12 are also important.

It is interesting to note that the idea of hole pairs moving through the RVB background seems to more accurately represent the ground state of the t-J model than the Hubbard model. Using the well-known relation at strong coupling, $J \approx 4t^2/U$, the RVA agrees to within 92% of the true ground-state energy of the t-J ladder for $J=0.5$ ($U=8$) at a doping of $x=\frac{1}{8}$. There are two ways to interpret this; either the t-J model supports pairing better than the Hubbard model, or we must view the hole pairs in the Hubbard model as having a larger size (i.e., larger coherence length).

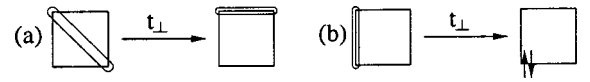

FIG. 13. For $t \ll t_\perp$, hopping along the rung dominates. By putting the particles (or holes) on adjacent rungs, we can have the situation shown in (a). However, by putting both particles (or holes) on the same rung, we get the situation shown in (b), which is energetically unfavorable.

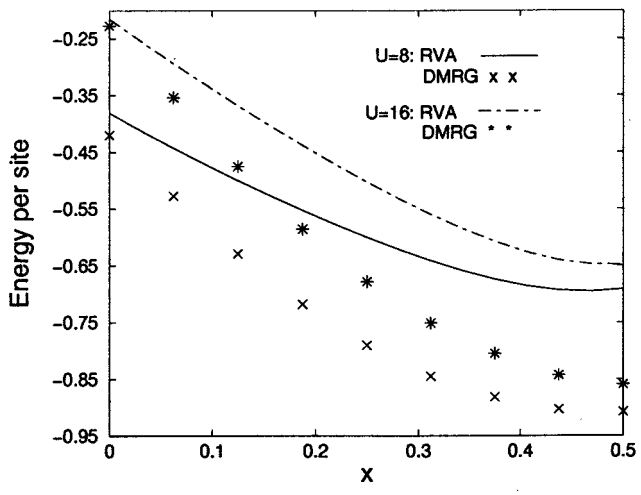

FIG. 14. Ground-state energy per site vs doping for a 2×32 ladder (with $t=t_\perp=1$) for $U=8$ (solid line) and $U=16$ (dashed-dotted line). For comparison, DMRG results for $U=8$ ($\times$) and $U=16$ (*) are shown.

V. CONCLUDING REMARKS

To summarize, we applied the recurrent variational approach to the two-leg Hubbard ladder. Our results were in qualitative agreement with previous results on the Heisenberg and t-J ladders. For the half-filled ladder, the generalized RVB state became more accurate in the parameter regime where the Hubbard and Heisenberg ladders were shown to coincide. However, comparison of the RVA with DMRG for the doped ladder indicates that hole pairs moving through an RVB background is incomplete. ''Pair-breaking'' configurations are also necessary to capture the essential physics.

As we saw, the strength of the RVA is the ease in which we could extract the physics. We were able to see the importance of the configurations in our ansatz quite easily. Furthermore, the RVA has a natural way in which to include longer bonds in the ansatz to more accurately represent the ground-state wave function. The importance of such additional states to the physics of the ladder is not easily probed with other techniques.

Generalized RVB states similar to ours have been considered previously for the half-filled Hubbard ladder.[23] Fano *et al.* were even able to produce an ansatz coming within 98% of the true ground state energy for a (half filled) 2×4 ladder at $U=16$. (Their ansatz included diagonal bonds of length $\sqrt{5}$.) However, none of these works considered the doped case. Using the approach in Ref. 17 (in terms of dimer coverings), it appears to be a formidable task to consider doping. This is one of the strengths of the RVA; doping is handled rather easily. Even though our results for the doped ladder showed that hole pairs moving through an RVB back-

ground is incomplete, the RVA offers a straightforward way to improve the situation, namely include ''pair-breaking'' configurations (shown in Fig. 12) in the ansatz.

Another (and probably better) way to improve the situation for the doped ladder is to consider a matrix product ansatz.[24,25] A matrix product ansatz can be generated by first order recursion relations.[25] In the RVA, the size of the hole pairs are fixed. (In our case, the hole pairs had a size of one lattice spacing.) However, by construction, the matrix product ansatz takes into account hole pairs of *arbitrary* size. We leave this (and other possibilities) for future work.

ACKNOWLEDGMENTS

We would like to thank D. J. Scalapino, S. Daul, S. Hortikar, R. Konik, C. L. Martin, and M. A. Martin-Delgado for helpful discussions and comments. E.H.K. gratefully acknowledges the warm hospitality of Argonne National Laboratory where parts of this manuscript were written. D.D. would like to thank S. Daul and R. M. Noack for assistance with the DMRG results presented here. E.H.K. was supported by NSF Grant No. DMR-9527304, G.S. by DGES Grant No. PB97-1190, and D.D. by DOE Grant No. DE-FG03-85ER451907.

APPENDIX A: THE HALF-FILLED LADDER

The states in the ansatz for the half-filled ladder of Eq. (6) are given by

$$
\begin{aligned}
|\phi_0\rangle_{N+2} &= \Delta^\dagger_{(N+2,1),(N+2,2)}|0\rangle_{N+2},\\
|\phi_1\rangle_{N+2} &= D^\dagger_{(N+2,1)}|0\rangle_{N+2}+D^\dagger_{(N+2,2)}|0\rangle_{N+2},\\
|\phi_2\rangle_{N+1,N+2} &= \Delta^\dagger_{(N+1,1),(N+2,1)}\Delta^\dagger_{(N+1,2),(N+2,2)}|0\rangle_{N+1,N+2},\\
|\phi_3\rangle_{N+1,N+2} &= D^\dagger_{(N+1,1)}D^\dagger_{(N+1,2)}|0\rangle_{N+1,N+2}+D^\dagger_{(N+2,1)}D^\dagger_{(N+2,2)}|0\rangle_{N+1,N_2},\\
|\phi_4\rangle_{N+1,N+2} &= \Delta^\dagger_{(N+1,1),(N+2,1)}D^\dagger_{(N+1,2)}|0\rangle_{N+1,N+2}+\Delta^\dagger_{(N+1,1),(N+2,1)}D^\dagger_{(N+2,2)}|0\rangle_{N+1,N+2}\\
&\quad+\Delta^\dagger_{(N+1,2),(N+2,2)}D^\dagger_{(N+1,1)}|0\rangle_{N+1,N+2}+\Delta^\dagger_{(N+1,2),(N+2,2)}D^\dagger_{(N+2,1)}|0\rangle_{N+1,N+2},\\
|\phi_5\rangle_{N+1,N+2} &= D^\dagger_{(N+1,1)}D^\dagger_{(N+2,2)}|0\rangle_{N+1,N+2}+D^\dagger_{(N+1,2)}D^\dagger_{(N+2,1)}|0\rangle_{N+1,N+2},\\
|\phi_6\rangle_{N,N+1,N+2} &= \Delta^\dagger_{(N,1),(N+2,2)}\Delta^\dagger_{(N+1,1),(N+2,1)}D^\dagger_{(N,2)}|0\rangle_{N,N+1,N+2}+\Delta^\dagger_{(N,1),(N+2,2)}\Delta^\dagger_{(N+1,1),(N+2,1)}D^\dagger_{(N+1,2)}|0\rangle_{N,N+1,N+2}\\
&\quad+\Delta^\dagger_{(N,2),(N+2,1)}\Delta^\dagger_{(N+1,2),(N+2,2)}D^\dagger_{(N,1)}|0\rangle_{N,N+1,N+2}+\Delta^\dagger_{(N,2),(N+2,1)}\Delta^\dagger_{(N+1,2),(N+2,2)}D^\dagger_{(N+1,1)}|0\rangle_{N,N+1,N+2},\\
|\phi_7\rangle_{N,N+1,N+2} &= \Delta^\dagger_{(N,1),(N+2,2)}\Delta^\dagger_{(N,2),(N+1,2)}D^\dagger_{(N+1,1)}|0\rangle_{N,N+1,N+2}+\Delta^\dagger_{(N,1),(N+2,2)}\Delta^\dagger_{(N,2),(N+1,2)}D^\dagger_{(N+2,1)}|0\rangle_{N,N+1,N+2}\\
&\quad+\Delta^\dagger_{(N,2),(N+2,1)}\Delta^\dagger_{(N,1),(N+1,1)}D^\dagger_{(N+1,2)}|0\rangle_{N,N+1,N+2}+\Delta^\dagger_{(N,2),(N+2,1)}\Delta^\dagger_{(N,1),(N+1,1)}D^\dagger_{(N+2,2)}|0\rangle_{N,N+1,N+2}.
\end{aligned}
\tag{A1}
$$

To derive the recursion relations, the following inner products are necessary:

$$
\begin{gathered}
{}_{N+2}\langle\phi_0|\phi_0\rangle_{N+2}=2,\ {}_{N+2}\langle\phi_1|\phi_1\rangle_{N+2}=2,\ {}_{N+1,N+2}\langle\phi_2|\phi_2\rangle_{N+1,N+2}=4,\\
{}_{N+1,N+2}\langle\phi_3|\phi_3\rangle_{N+1,N+2}=2,\ {}_{N+1,N+2}\langle\phi_4|\phi_4\rangle_{N+1,N+2}=8,\ {}_{N+1,N+2}\langle\phi_5|\phi_5\rangle_{N+1,N+2}=2,\\
{}_{N,N+1,N+2}\langle\phi_6|\phi_6\rangle_{N,N+1,N+2}=16,\ {}_{N,N+1,N+2}\langle\phi_7|\phi_7\rangle_{N,N+1,N+2}=16,\\
\langle N+1|_{N+2}\langle\phi_0|\phi_2\rangle_{N+1,N+2}|N\rangle=(-1)\langle N+1|\phi_0\rangle_{N+1}|N\rangle,\\
\langle N+1|_{N+2}\langle\phi_1|\phi_5\rangle_{N+1,N+2}|N\rangle=\langle N+1|\phi_1\rangle_{N+1}|N\rangle,\\
\langle N+1|_{N+2}\langle\phi_0|\phi_6\rangle_{N,N+1,N+2}|N-1\rangle=(-1)\langle N+1|\phi_4\rangle_{N,N+1}|N-1\rangle,\\
\langle N|_{N+1,N+2}\langle\phi_4|\phi_7\rangle_{N,N+1,N+2}|N-1\rangle=(-4)\langle N|\phi_0\rangle_N|N-1\rangle.
\end{gathered}
\tag{A2}
$$

Using these inner products, a straightforward calculation gives the following (coupled) recursion relations:

$$
\begin{aligned}
Z_{N+2} &= (2+2\alpha^2)Z_{N+1}-2\beta Y_{N+1}+2\alpha\eta X_{N+1}+(4\beta^2+2\gamma^2+8\xi^2+2\eta^2)Z_N+(16\delta^2+16\varepsilon^2-16\xi\delta)Z_{N-1}-8\xi\varepsilon Y_N\\
&\quad+8\delta\varepsilon Y_{N-1},
\end{aligned}
$$

$$
\begin{aligned}
Y_{N+2}&=2Z_{N+1}-\beta Y_{N+1}-8\xi\delta Z_{N-1}+4\delta\varepsilon Y_{N-1},\\
X_{N+2}&=2\alpha Z_{N+1}+\eta X_{N+1},\\
E_{N+2}&=(2+2\alpha^2)E_{N+1}+(-8t_\perp\alpha+2U\alpha^2)Z_{N+1}-2\beta D_{N+1}+2\alpha\eta C_{N+1}+(8t\xi+4t_\perp\alpha\beta)Y_{N+1}+(-4t_\perp\eta-8t\alpha\xi\\
&\quad+2U\alpha\eta)X_{N+1}+(4\beta^2+2\gamma^2+8\xi^2+2\eta^2)E_N+(-32t\beta\xi+4U\gamma^2-16t\gamma\xi+8U\xi^2-16t\xi\eta+4U\eta^2)Z_N+(16t\beta\delta\\
&\quad-8t\varepsilon+8t\alpha^2\varepsilon+16t\beta\varepsilon+8t\gamma\varepsilon-8U\xi\varepsilon+8t\eta\varepsilon-8t\delta)Y_N+8t\alpha\delta X_N+(32t\beta\varepsilon+16U\delta^2+16U\varepsilon^2+32t\beta\delta+16t\gamma\delta\\
&\quad-16U\xi\delta+16t\eta\delta+32t_\perp\alpha\delta\xi)X_{N-1}-8\xi\varepsilon D_N+(16\delta^2+16\varepsilon^2-16\delta\xi)E_{N-1}+8\delta\varepsilon D_{N-1}+(8U\delta\varepsilon-16t_\perp\alpha\delta\varepsilon)Y_{N-1},\\
D_{N+2}&=2E_{N+1}-4t_\perp\alpha Z_{N+1}-\beta D_{N+1}+4t\xi Y_{N+1}-2t_\perp\eta X_{N+1}+(-4t\varepsilon-4t\delta)Y_N+4t\alpha\delta X_N+(16t\beta\delta+8t\gamma\delta-8U\xi\delta\\
&\quad+8t\eta\delta+16t\beta\varepsilon)Z_{N-1}-8\xi\delta E_{N-1}+4\delta\varepsilon D_{n-1}+4U\delta\varepsilon Y_{N-1},\\
C_{N+2}&=2\alpha E_{N+1}+(-4t_\perp+2U\alpha)Z_{N+1}+2t_\perp\beta Y_{N+1}+(-4t\xi+U\eta)X_{N+1}+\eta C_{N+1}+16t_\perp\xi\delta Z_{N-1}-8t_\perp\delta\varepsilon Y_{N-1}+4t\alpha\varepsilon Y_N.
\end{aligned}
\tag{A3}
$$

APPENDIX B: THE DOPED LADDER

For the doped ladder [see Eq. (11)], $|\phi_0\rangle_{N+2}$, $|\phi_1\rangle_{N+2}$, $|\phi_2\rangle_{N+1,N+2}$, $|\phi_3\rangle_{N+1,N+2}$, $|\phi_4\rangle_{N+1,N+2}$, $|\phi_5\rangle_{N+1,N+2}$, $|\phi_6\rangle_{N,N+1,N+2}$, and $|\phi_7\rangle_{N,N+1,N+2}$ are the same as the half-filled case, and

$$
\begin{aligned}
|\phi_0^h\rangle_{N+2}&=|0\rangle_{N+2},\\
|\phi_1\rangle_{N+1,N+2}&=\Delta^\dagger_{(N+1,1),(N+2,2)}|0\rangle_{N+1,N+2}+\Delta^\dagger_{(N+2,1),(N+1,2)}|0\rangle_{N+1,N+2},\\
|\phi_2\rangle_{N+1,N+2}&=\Delta^\dagger_{(N+1,1),(N+2,1)}|0\rangle_{N+1,N+2}+\Delta^\dagger_{(N+1,2),(N+2,2)}|0\rangle_{N+1,N+2},\\
|\phi_3\rangle_{N,N+1,N+2}&=\Delta^\dagger_{(N,1),(N+2,1)}\Delta^\dagger_{(N+1,2),(N+2,2)}|0\rangle_{N,N+1,N+2}+\Delta^\dagger_{(N,2),(N+2,2)}\Delta^\dagger_{(N+1,1),(N+2,1)}|0\rangle_{N,N+1,N+2},\\
|\phi_4\rangle_{N,N+1,N+2}&=\Delta^\dagger_{(N,1),(N+2,1)}\Delta^\dagger_{(N,2),(N+1,2)}|0\rangle_{N,N+1,N+2}+\Delta^\dagger_{(N,2),(N+2,2)}\Delta^\dagger_{(N,1),(N+1,1)}|0\rangle_{N,N+1,N+2}.
\end{aligned}
\tag{B1}
$$

To derive the recursion relations, we use the inner products from the half-filled case as well as the the following:

$$
\begin{aligned}
&{}_{N+2}\langle\phi_0^h|\phi_0^h\rangle_{N+2}=1,\ {}_{N+1,N+2}\langle\phi_1^h|\phi_1^h\rangle_{N+1,N+2}=4,\ {}_{N+1,N+2}\langle\phi_2^h|\phi_2^h\rangle_{N+1,N+2}=4,\\
&{}_{N,N+1,N+2}\langle\phi_3^h|\phi_3^h\rangle_{N,N+1,N+2}=8,\ {}_{N,N+1,N+2}\langle\phi_4^h|\phi_4^h\rangle_{N,N+1,N+2}=8,\\
&\langle N+1P+1|_{N+2}\langle\phi_0|\phi_3^h\rangle_{N,N+1,N+2}|N-1P\rangle=(-1)\langle N+1P+1|\phi_1^h\rangle_{N,N+1}|N-1P\rangle,\\
&\langle NP|_{N+1,N+2}\langle\phi_1^h|\phi_4^h\rangle_{N,N+1,N+2}|N-1P\rangle=(-2)\langle NP|\phi_0\rangle_N|N-1P\rangle.
\end{aligned}
\tag{B2}
$$

Using these inner products, a straightforward calculation gives the following (coupled) recursion relations:

$$
\begin{aligned}
Z_{N+2,P+1}&=(2+2\alpha^2)Z_{N+1,P+1}-2\beta Y_{N+1,P+1}+2\alpha\eta X_{N+1,P+1}+(4\beta^2+2\gamma^2+8\xi^2+2\eta^2)Z_{N,P+1}+(16\delta^2+16\varepsilon^2\\
&\quad-16\xi\delta)Z_{N-1,P+1}-8\xi\varepsilon Y_{N,P+1}+8\delta\varepsilon Y_{N-1,P+1}+Z_{N+1,P}+(4\lambda^2+4\zeta^2)Z_{N,P}-4\lambda\nu Y_{N,P}+(8\mu^2+8\nu^2\\
&\quad-8\lambda\mu)Z_{N-1,P}+4\mu\nu Y_{N-1,P},\\
Y_{N+2,P+1}&=2Z_{N+1,P+1}-\beta Y_{N+1,P+1}-8\xi\delta Z_{N-1,P+1}+4\delta\varepsilon Y_{N-1,P+1}-4\mu\lambda Z_{N-1,P}+2\mu\nu Y_{N-1,P},\\
X_{N+2,P+1}&=2\alpha Z_{N+1,P+1}+\eta X_{N+1,P+1},\\
E_{N+2,P+1}&=(2+2\alpha^2)E_{N+1,P+1}+(-8t_\perp\alpha+2U\alpha^2)Z_{N+1,P+1}-2\beta D_{N+1,P+1}+2\alpha\eta C_{N+1,P+1}+(8t\xi+4t_\perp\alpha\beta)Y_{N+1,P+1}\\
&\quad+(-4t_\perp\eta-8t\alpha\xi+2U\alpha\eta)X_{N+1,P+1}+(4\beta^2+2\gamma^2+8\xi^2+2\eta^2)E_{N,P+1}+(-32t\beta\xi+4U\gamma^2-16t\gamma\xi+8U\xi^2\\
&\quad-16t\xi\eta+4U\eta^2)Z_{N,P+1}+(16t\beta\delta-8t\varepsilon+8t\alpha^2\varepsilon+16t\beta\varepsilon+8t\gamma\varepsilon-8U\xi\varepsilon+8t\eta\varepsilon-8t\delta)Y_{N,P+1}+8t\alpha\delta X_{N,P+1}\\
&\quad+(32t\beta\varepsilon+16U\delta^2+16U\varepsilon^2+32t\beta\delta+16t\gamma\delta-16U\xi\delta+16t\eta\delta+32t_\perp\alpha\delta\xi)X_{N-1,P+1}-8\xi\varepsilon D_{N,P+1}+(16\delta^2\\
&\quad+16\varepsilon^2-16\delta\xi)E_{N-1,P+1}+8\delta\varepsilon D_{N-1,P+1}+(8U\delta\varepsilon-16t_\perp\alpha\delta\varepsilon)Y_{N-1,P+1}+E_{N+1,P}+(4\lambda^2+4\zeta^2)E_{N,P}+(8\mu^2\\
&\quad+8\nu^2-8\lambda\mu)E_{N-1,P}-4t\lambda Y_{N+1,P}-4t\zeta X_{N+1,P}+(-16t_\perp\lambda\zeta-8t\lambda-8t\alpha\zeta)Z_{N,P}+(4t\nu+8t_\perp\zeta\nu+4t\mu+4t\nu)Y_{N,P}
\end{aligned}
\tag{B3}
$$

$$+(-16t\beta\nu+8t\mu+16t_\perp\zeta\mu+16t_\perp\alpha\lambda\mu-16t\beta\mu)Z_{N-1,P}-4\lambda\nu D_{N,P}+4\mu\nu D_{N-1,P}-8t_\perp\alpha\mu\nu Y_{N-1,P},$$

$$D_{N+2,P+1}=2E_{N+1,P+1}-4t_\perp\alpha Z_{N+1,P+1}-\beta D_{N+1,P+1}+4t\xi Y_{N+1,P+1}-2t_\perp\eta X_{N+1,P+1}+(-4t\varepsilon-4t\delta)Y_{N,P+1}$$
$$+4t\alpha\delta X_{N,P+1}+(16t\beta\delta+8t\gamma\delta-8U\xi\delta+8t\eta\delta+16t\beta\varepsilon)Z_{N-1,P+1}-8\xi\delta E_{N-1,P+1}+4\delta\varepsilon D_{N-1,P+1}$$
$$+4U\delta\varepsilon Y_{N-1,P+1}-4t\lambda Z_{N,P}+(2t\nu+2t\mu)Y_{N,P}-4\lambda\mu E_{N-1,P}+2\mu\nu D_{N-1,P}+(4t\mu+8t_\perp\zeta\mu)Z_{N-1,P},$$

$$C_{N+2,P+1}=2\alpha E_{N+1,P+1}+(-4t_\perp+2U\alpha)Z_{N+1,P+1}+2t_\perp\beta Y_{N+1,P+1}+(-4t\xi+U\eta)X_{N+1,P+1}+\eta C_{N+1,P+1}$$
$$+16t_\perp\xi\delta Z_{N-1,P+1}-8t_\perp\delta\varepsilon Y_{N-1,P+1}+4t\alpha\varepsilon Y_{N,P+1}-4t\zeta Z_{N,P}+8t_\perp\lambda\mu Z_{N-1,P}-4t_\perp\mu\nu Y_{N-1,P}.$$

[1] For a review see E. Dagotto and T. M. Rice, Science **271**, 618 (1996).

[2] For example, see C. Varma and A. Zawadowski, Phys. Rev. B **32**, 7399 (1985); D. G. Shelton, A. A. Nerseynan, and A. M. Tsvelik, *ibid.* **53**, 8521 (1996); H. H. Lin, L. Balents, and M. P. A. Fisher, *ibid.* **58**, 1794 (1998), and references therein.

[3] For example, see T. M. Rice, S. Haas, M. Sigrist, and F. C. Zhang, Phys. Rev. B **56**, 14 655 (1997); R. M. Noak, S. R. White, and D. J. Scalapino, Physica C **270**, 281 (1996), and references therein.

[4] Z. Hiroi, M. Azuma, M. Takano, and Y. Bando, J. Solid State Chem. **95**, 230 (1991); M. Uehara, T. Nagata, J. Akimitsu, H. Takahashi, N. Môri, and K. Kinoshita, J. Phys. Soc. Jpn. **65**, 2764 (1996), and references therein.

[5] D. C. Johnston, J. W. Johnson, D. P. Goshorn, and A. J. Jacobson, Phys. Rev. B **35**, 219 (1987); R. S. Eccleston, T. Barnes, J. Brody, and J. W. Johnson, Phys. Rev. Lett. **73**, 2626 (1994).

[6] Z. Hiroi, M. Azuma, M. Takano, and Y. Bando, J. Solid State Chem. **95**, 230 (1991); M. Azuma, Z. Hiroi, M. Takano, K. Ishida, and Y. Kitaoka, Phys. Rev. Lett. **73**, 3463 (1994).

[7] M. Azuma *et al.*, Phys. Rev. Lett. **73**, 3463 (1994).

[8] G. Sierra and M. A. Martin-Delgado, Phys. Rev. B **56**, 8774 (1997).

[9] G. Sierra, M. A. Martin-Delgado, J. Dukelsky, S. R. White, and D. J. Scalapino, Phys. Rev. B **57**, 11 666 (1998).

[10] M. A. Martin-Delgado and G. Sierra, in *Density Matrix Renormalization*, edited by I. Peschel *et al.* (Springer-Verlag, Berlin, 1999).

[11] K. G. Wilson, Rev. Mod. Phys. **47**, 773 (1975).

[12] S. R. White, Phys. Rev. Lett. **69**, 2863 (1992); Phys. Rev. B **48**, 10 345 (1993).

[13] S. R. White, R. M. Noack, and D. J. Scalapino, Phys. Rev. Lett. **73**, 886 (1994).

[14] J. Piekarewicz and J. R. Shepard, Phys. Rev. B **56**, 5366 (1997).

[15] E. Dagotto, G. B. Martins, J. Riera, A. L. Malvezzi, and C. Gazza, Phys. Rev. B **58**, 12 063 (1998).

[16] J. Piekarewicz and J. R. Shepard, Phys. Rev. B **58**, 9326 (1998).

[17] For example, see C. Y. Pan and Xiyao Chen, Phys. Rev. B **36**, 8600 (1987); M. D. Kovarik, *ibid.* **41**, 6889 (1990); J. E. Hirsch, *ibid.* **22**, 5259 (1980); C. Dasgupta and P. Pfeuty, J. Phys. C **14**, 717 (1981), and references therein.

[18] Note that $|\phi_i\rangle_{N+2,N+1}|N\rangle$ should (more precisely) be written $|\phi_i\rangle_{N+2,N+1}\otimes|N\rangle$. However, throughout the paper, to make things less notationally cumbersome, we have omitted the tensor product symbol.

[19] D. J. Scalapino and S. A. Trugman, Philos. Mag. B **74**, 607 (1996).

[20] S. R. White and D. J. Scalapino, Phys. Rev. B **55**, 6504 (1997).

[21] S. Daul and R. M. Noack (private communication).

[22] E. Jeckelmann, D. J. Scalapino, and S. R. White, Phys. Rev. B **58**, 9492 (1998).

[23] G. Fano, F. Ortolani, and L. Ziosi, Phys. Rev. B **54**, 17 557 (1996); A. Messager and J. L. Richard, Phys. Lett. A **143**, 345 (1990); G. M. Cicuta and S. Stramaglia, *ibid.* **165**, 456 (1992).

[24] S. Östlund and S. Rommer, Phys. Rev. Lett. **75**, 3537 (1995); S. Östlund and S. Rommer, Phys. Rev. B **55**, 2164 (1997).

[25] J. M. Roman, G. Sierra, J. Dukelsky, and M. A. Martin-Delgado, J. Phys. A **31**, 9729 (1998).